

Hard Magnetic Elastomers Incorporating Magnetic Annealing and Soft Magnetic Particulate for Fused Deposition Modeling

Sarah J. Ziemann¹, Nathan A. Fischer¹, Jimmy Lu¹, Thomas J. Lee¹, Michael Ennis¹, Thomas A. Höft², and Brittany Nelson-Cheeseman¹

¹Department of Mechanical Engineering, University of St. Thomas, St. Paul, MN 55105, USA

²Department of Mathematics, University of St. Thomas, St. Paul, MN 55105, USA

Sarah Ziemann, corresponding author, sarahziemann@gmail.com

I. Abstract

Magnetic elastomers with hard or permanent magnetic particulate are able to achieve complex motion not possible from soft magnetic elastomers. Magnetic annealing and fused deposition modeling (FDM) have been used to increase the performance of magnetic composites. This research explores how the magnetoactive properties of hard magnetic elastomers are influenced by magnetic annealing and the addition of the soft magnetic particulate. Three compositions of thermoplastic magnetic elastomer composite are explored: 15 vol% SrFe₁₂O₁₉, 10 vol% SrFe₁₂O₁₉/5 vol% carbonyl iron, and 5 vol% SrFe₁₂O₁₉/10 vol% carbonyl iron. The material is then extruded into FDM filaments. During the extrusion process, some filament is magnetically annealed in an axial applied field. Magnetic hysteresis loops show that the saturation magnetization and coercivity change based on the relative amount of hard and soft magnetic particulate. The presence of only one coercive field indicates magnetic coupling between the hard and soft components. Magnetoactive testing measures each sample's mechanical deflection angle as a function of transverse applied magnetic field strength. Qualitative and quantitative results reveal that magnetic annealing is critical to the magnetoactive performance of the hard magnetic elastomers. The results also demonstrate that magnetic annealing and increased carbonyl iron both improve the magnetoactive deflection angle for a given applied field. Scanning electron microscopy shows a stratification effect in a range of the filaments. Understanding these hard magnetic elastomers provides insight into how performance can be controlled and optimized by magnetic annealing and combining hard and soft magnetic particulate.

II. Introduction

Magnetic elastomers are smart materials that can deform, stretch, and change shape based on the application of a magnetic field.^{1,2,3,4,5} They are often composites, consisting of a polymer material and magnetic particulate. These magnetic elastomers can have a variety of applications in soft robotics and biomedical engineering, where achieving high deformation of a material remotely is critical to its success.⁶ An example of this application is artificial muscles.^{1,7}

Magnetic elastomers perform best when there is increased anisotropy within the composite.⁸ The material then has different properties along different axes, which allows for more control over the shape and movement of the material.⁹ Various methods and processing techniques can affect the anisotropy of the material, including using magnetic annealing and fused deposition modeling (FDM).^{10,11}

Magnetic annealing has been shown to improve the anisotropy of magnet composites.^{11,12,13} Preferentially aligning a magnetic material along an applied field axis decreases the applied magnetic field that is needed to magnetize the material along its “easy axis.” This anisotropic effect is created from the structural changes that occur, and the effect improves the material’s overall performance.¹¹

Creating anisotropy is also possible through Fused Deposition Modeling (FDM), also known as 3D printing. FDM is a particularly promising 3D printing process because it involves extruding material into 1D lines, which gives more control over the mesoscale anisotropy of the internal structure of certain parts.¹⁴ Besides increasing the control over overall anisotropy, FDM allows the fabrication of magnetic elastomers to be more accessible.^{14, 15} It also does not require curing, cross-linking, or post-processing.¹⁴

Previous studies of magnetic elastomers used for FDM focused on using a magnetically soft or impermanent particulate, such as carbonyl iron or magnetite (Fe_3O_4).^{10, 11, 14} Using a magnetically hard or permanent particulate, such as strontium ferrite ($\text{SrFe}_{12}\text{O}_{19}$), may reveal interesting or improved performance of the magnetic elastomers because hard magnets react with magnetic fields differently than soft magnets.¹⁶ Research on hard magnetic elastomers reveals that these smart materials can exhibit more complex motion, such as rolling, twisting, and folding, than soft magnetic elastomers, which makes them exceptional actuators.^{16,17,18,19,20,21,22,23} Strontium ferrite is a particularly important hard magnetic particulate material because it is cheaper than neodymium magnets (NdFeB), and it has been successfully utilized in related polymer composite materials.^{9,24,25,26,27} Another area of improvement in performance may be a combination of a soft magnet, such as carbonyl iron, and a hard magnet, such as strontium ferrite, to create a hybrid magnetic elastomer with the best properties of both of the magnets. Magnetic coupling effects within the hybrid elastomer could allow for multi-functional applications, combining the flexible motion of soft magnetic elastomers with the more complex motion of hard magnetic elastomers.^{12, 28}

This research study seeks to create and analyze filament with permanent (hard) and mixed (soft and hard) magnetic particulate that has been magnetically annealed for use in 3D printing via Fused Deposition Modeling (FDM). Combining hard and soft magnets provides exciting opportunities to increase the anisotropy within the filament and to maximize the best properties of different types of magnets. Magnetic annealing also provides interesting ways to increase performance and anisotropy. Both permanent magnets and magnetic annealing are used to maximize performance of magnetic elastomers that can be 3D printed, which have ample applications in soft robotics and biomedical engineering.

III. Methods

A. Materials and sample types

NinjaFlex® thermoplastic polyurethane pellets, with a listed melting point of 216°C, were used. Dimethylformamide (DMF) is used as a solvent for the pellets. Strontium ferrite (SrF) particulate (1.1-1.4 microns) was obtained from Dowa Electronics Materials. Carbonyl iron (Fe) particulate (1-3 microns) was also used.

For this analysis, Table I shows the samples created based on the amount of strontium ferrite (SrF) and carbonyl iron (Fe) used and whether the samples were magnetically annealed or not.

Sample name	%vol SrF	%vol Fe	Magnetic Annealing (number of magnets)
15SrF-0M	15	0	No (0M)
15SrF-5M	15	0	Yes (5M)
10SrF-5 Fe-0M	10	5	No (0M)
10SrF-5 Fe-5M	10	5	Yes (5M)
5SrF-10Fe-0M	5	10	No (0M)
5SrF-10Fe-5M	5	10	Yes (5M)

Table I Samples Chart

B. Solvent casting

Following the work of Lee et al., NinjaFlex pellets were dissolved in DMF solvent with a material to solvent ratio of 1:5.²⁹ After the pellets are fully dissolved, the magnetic particulate of a determined volume percentage is stirred into the solution. The solution is poured into silicone trays and placed in a dehydrator for at least 72 hours to evaporate the solvent.

C. Extrusion

After the material is dried, it is cut into small pieces (around 1 cm x 2 cm). It is then fed through a Filabot EX2 extruder. The filament is extruded at 186°C using a 2 mm diameter nozzle, as detailed by Fischer et al.¹¹

D. Magnetic annealing

Magnetic annealing also follows the methods developed in Fischer et al.¹¹ The samples are fed through the Filabot EX2 and the permanent magnet (NdFeB) stand directly after extrusion. The samples detailed in this research are “5 M” samples, meaning that they are passed through a uniform axial applied magnetic field created with four sets of 5 NdFeB magnets in a stack. The extrudate is gently pulled as it is extruding, contrasting the die swell effect that occurs at the nozzle head.¹¹

E. Testing Methods

To understand the magnetic properties of the filaments, a vibrating sample magnetometer (VSM) with a range of ± 1.9 T was used to determine the properties and shape of the hysteresis loops of the different samples. Three samples of each type were used for magnetic testing, and each sample was tested with the applied field parallel (axial) and perpendicular (transverse) to the filament axis. The samples were cut to approximately 2 mm in length, since the diameter of the filament is 2 mm. This created comparable cross-sections in the parallel and perpendicular directions.

Magnetoactive testing was performed by hanging a 5.08 cm (2-inch) sample of filament in a transverse electromagnet field that increases from 0 T to 0.4 T (seen in Figure 1 and following Fischer et. al.¹¹) Three samples of each type of filament were tested, making 18 samples in total.

A camera is used to capture images of the filament at each applied field step as it is deflecting due to the applied transverse magnetic field. Then, a MATLAB program is used to analyze each image to quantitatively measure the angle of deformation by determining the angle between the filament at 0 T and each applied field. The MATLAB code provides values in degrees representing the angle of deformation (θ) at each applied field (T) and overlay images of the filament at each applied field step.

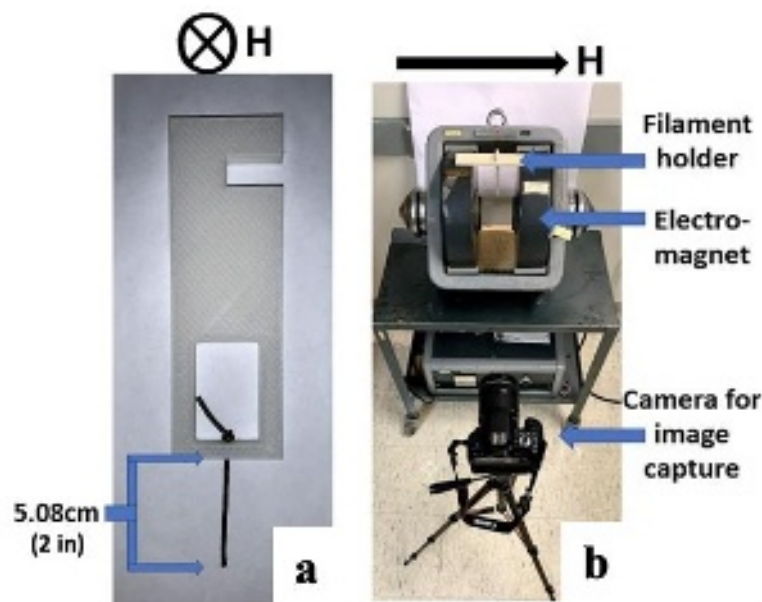


Figure 1 The entire magnetoactive testing set up. (a) 3D-printed structure used to hold the filament in place, and (b) camera and electromagnet used to apply a transverse electromagnetic field, indicated by H.

Scanning Electron Microscope (SEM) imaging obtains a better understanding of the underlying structure of the magnetic filaments. A JSM-IT200 SEM was used with a voltage of 15 keV to obtain images of the surface topography of the composite filament samples. These surface images help to study structural effects of magnetic annealing and different relative percentages of strontium ferrite and carbonyl iron.

IV. Results

A. Magnetic Properties

The axial and transverse hysteresis loops of all the filament types can be seen in Figure 2. The differing shapes of the hysteresis loops that arise from the relative amounts of hard and soft magnetic particulate can clearly be seen in Figure 2a. The pure strontium ferrite samples (15SrF) exhibit classic hard magnet behavior, showing a wide “square”-shape loop characterized by a large remnant magnetization (M_R) (M at $H=0$) and large coercive field (H_c) (H at $M=0$). The mixed samples have a progressively thinner shape with both lower remnant magnetizations and lower coercive fields. The lack of two distinct switching events for the mixed samples indicates that the two magnetic components are magnetically coupled to one another. The relative size of the remnant magnetization and coercive field indicates the ease of magnetic domain wall motion and magnetic moment rotation within the material. Larger values indicate more difficulty with

moving the domain walls or rotating the magnetic moments as is common in hard magnetic materials. Because strontium ferrite is a hard or permanent magnet, it is more difficult to change its magnetic alignment, while carbonyl iron is a soft or impermanent magnet, where it is much easier to move magnetic domain walls and change its magnetic alignment with the applied magnetic field. Additionally, the samples with higher relative carbonyl iron contents have larger saturation magnetization (M_s) at higher applied fields. This aligns with the larger M_s values of Fe compared to $\text{SrFe}_{12}\text{O}_{19}$.³⁰ For clarity, the maximum applied field in magnetoactive testing (0.4 T) is also shown with a red dashed line in Figure 2a and 2b.

Figure 2b shows the hysteresis loops of the filaments that have been magnetically annealed. Three samples of each type of filament were tested, and the median sample was used to compare hysteresis loops across compositions. The shapes of each type of filament are consistent with the non-magnetically annealed samples. While the 15SrF and 5SrF-10Fe samples appear very similar between both cases, the 10SrF-5Fe has a markedly different saturation magnetization. This could arise from inconsistencies in the particulate dispersion within the composite, possibly from magnetic clumping between the Fe and SrF due to the applied field during solidification. Nevertheless, the general unique shapes of the hysteresis loops are consistent.

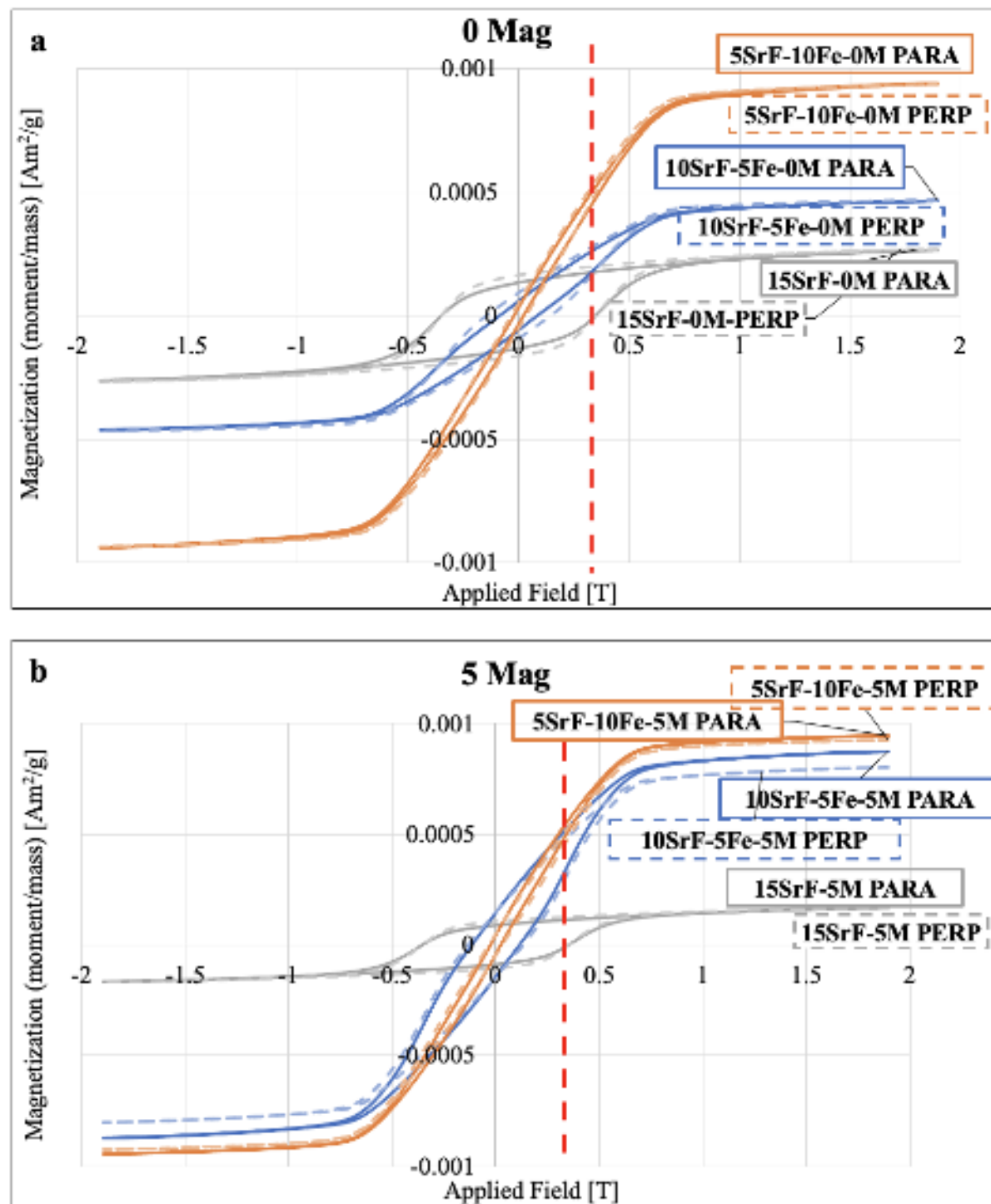


Figure 2 Hysteresis loops for (a) 0 M (no magnetic annealing) and (b) 5 M sample types (magnetic annealing).

B. Magnetoactive Properties

The magnetoactive images indicate the effectiveness of magnetic annealing, as demonstrated in Figure 3. Magnetic annealing greatly increases the magnetoactive response of the filament, as

seen when looking from left to right in Figure 3. This is especially critical in the pure strontium ferrite samples, as they have almost no magnetoactive response unless they are magnetically annealed. This underscores the critical nature of magnetic annealing for hard magnetic elastomers. Additionally, increasing the relative amount of iron in the sample increases the magnetoactive response of the filament at this maximum field of 0.4 T. The greatest response is shown in the 5SrF-10Fe-5Mag samples, which achieves the maximum deflection possible in this custom setup.

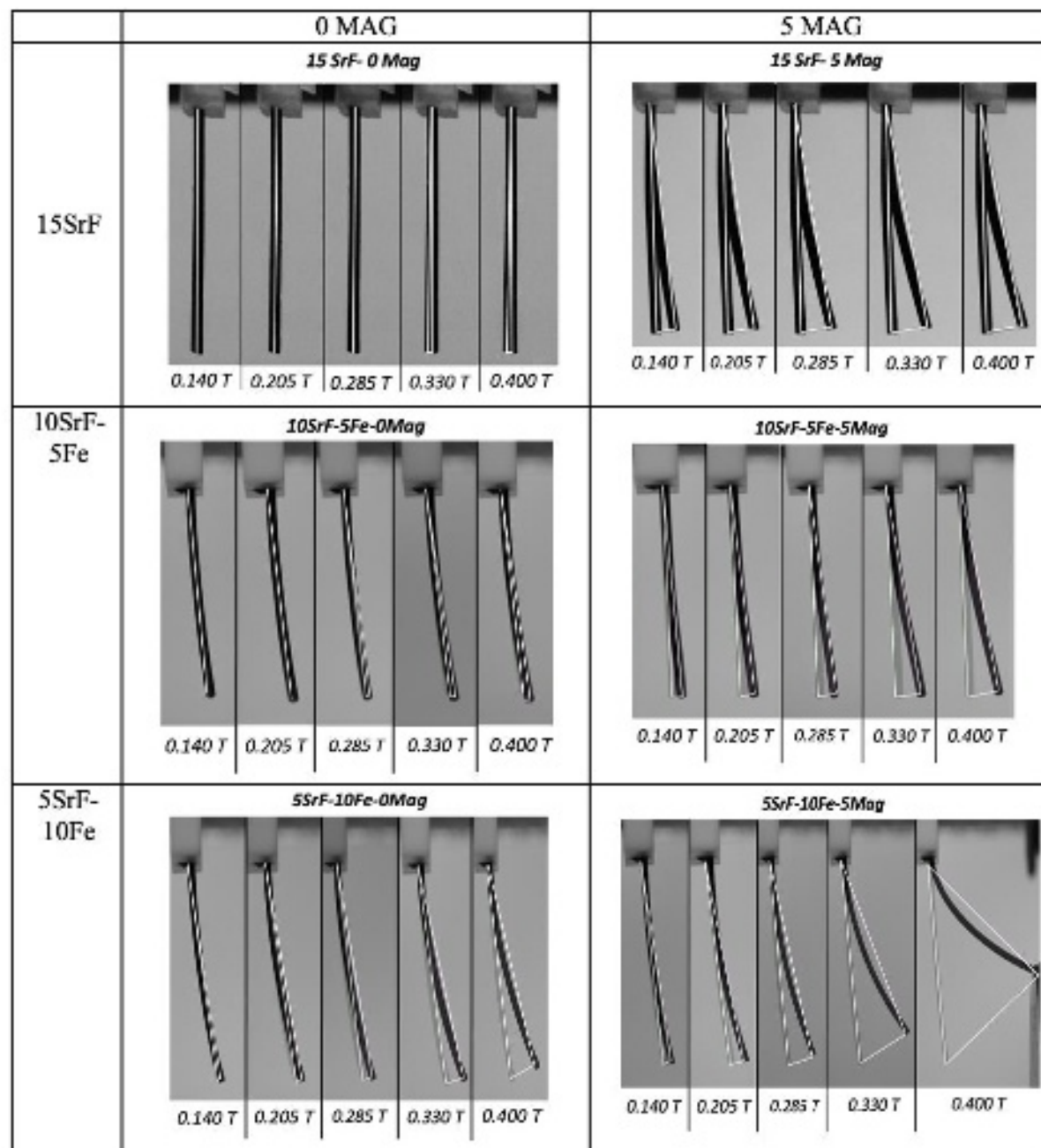


Figure 3 Magnetoactive images showing deformation of each sample type under increasing applied magnetic field. The images use an overlay of the deformed sample onto the sample with no applied field (0 T).

Figure 4 uses the MATLAB code to determine the angle of deformation of the deformed sample compared to the sample with no applied field. The results are then plotted to show the progression of angle of deformation with applied magnetic field. The image in the top left corner of each graph shows the image of the filament at its maximum angle of deflection.

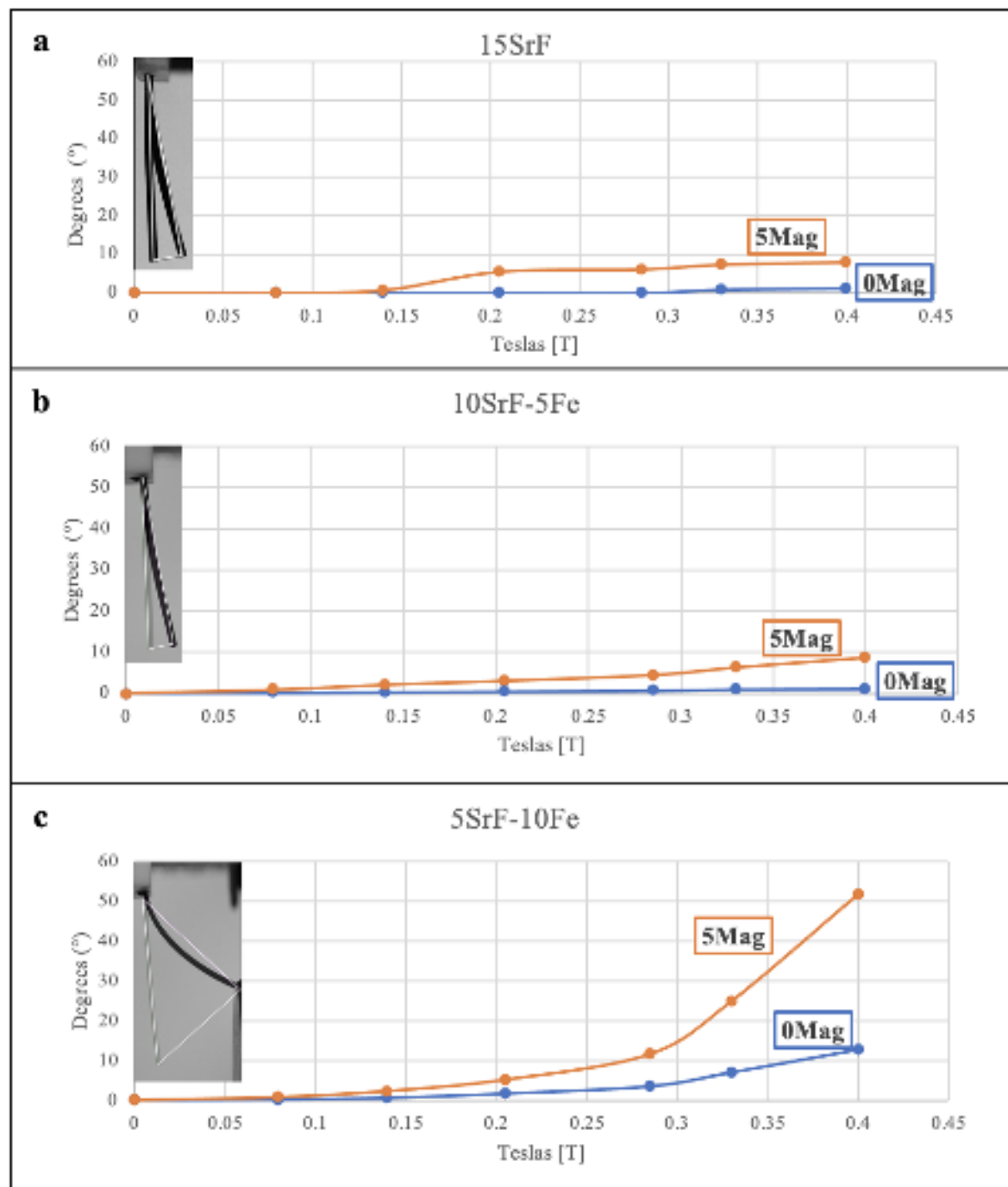


Figure 4 Angle of deformation of 0 M and 5 M sample under applied magnetic field for (a) 15 SrF, (b) 10SrF-5Fe, and (c) 5SrF-10Fe

The quantitative data from the magnetoactive images reinforces the qualitative data. The largest deformation is seen in the 5SrF-10Fe-5M sample, with its angle at 0.4 T being 52°. Due to the measurement configuration between the two electromagnets, the maximum deformation of the filament is approximately 50-55°. It is expected that the particulate within the filament is aligned in one direction along the longitudinal axis during the filament magnetic annealing process. In magnetic annealing, there is often either a rotation of the magnetic particulate to align with the applied magnetic annealing field (magnetically hard and/or anisotropically structured particulate) and/or a rearrangement of the particulate to create long chains that run parallel with the applied magnetic field (magnetically soft and/or isotropically structured particulate). The filament is then solidified to freeze the favored particulate arrangement in place. When a transverse magnetic field is applied during magnetoactive testing, the entire filament then moves more readily in the direction of that field due to the preferential alignment of the particulate already present within the filament. It is expected that the non-annealed samples would not have the same particulate alignment along the filament axis, so the filament does not respond as drastically to an applied magnetic field. In fact, for the hard magnetic particulate (15SrF), the lack of almost any magnetoaction for no magnetic annealing may be an indication of magnetically unaligned/randomized hard magnetic particulate. This would result in individual particulate magnets that compensate each other within the material and result in no net magnetic orientation to align with an applied external magnetic field. In this respect, magnetic annealing is critical to the performance of the hard magnetic elastomer materials.

The magnetic annealing response of these samples is consistent with the results of the 5 MAG samples in Fischer et. al.¹¹, in that using the “5 MAG” setup to align particulate creates greater magnetoactive response at lower fields for soft magnetic particulate. In Fischer et. al.,¹¹ the non-annealed iron samples eventually obtain the same angle of deformation as the annealed samples at 0.4 T, but the annealed samples have a greater response to an initial ramping up of magnetic field. The mixed samples with the largest amount of iron (5SrF-10Fe), regardless of magnetic annealing, show the greatest increase in angle of deflection as magnetic field increases. The 5SrF-10Fe-5M sample reaches the maximum angle of deflection possible for the measurement geometry. Based on Fischer et al.’s results, it is reasonable to suggest that the unannealed version (5SrF-10Fe-0M) would attain the same maximum magnetoactive deflection as its magnetically annealed counterpart if testing out to higher magnetic fields was possible.

C. Structural Imaging

SEM imaging helps to better analyze the micro- and meso-scale structure of the composite filaments. Figure 5 identifies the particulate within the thermoplastic polyurethane. The ball-shaped particulate within the sample is carbonyl iron, while the faceted or irregularly shaped pieces are strontium ferrite, as confirmed by Energy Dispersive Spectroscopy (EDS). The shape of the particulate could affect the overall anisotropy of the filament. The diamond-shaped strontium-ferrite particulate can align in different directions, as it has a different shape in different directions. The spherical-shaped carbonyl iron particulate is isotropic, meaning that its shape will be identical no matter the direction. Despite these shape anisotropy differences, no apparent difference in the relative orientation of these particulates within the filament could be found.

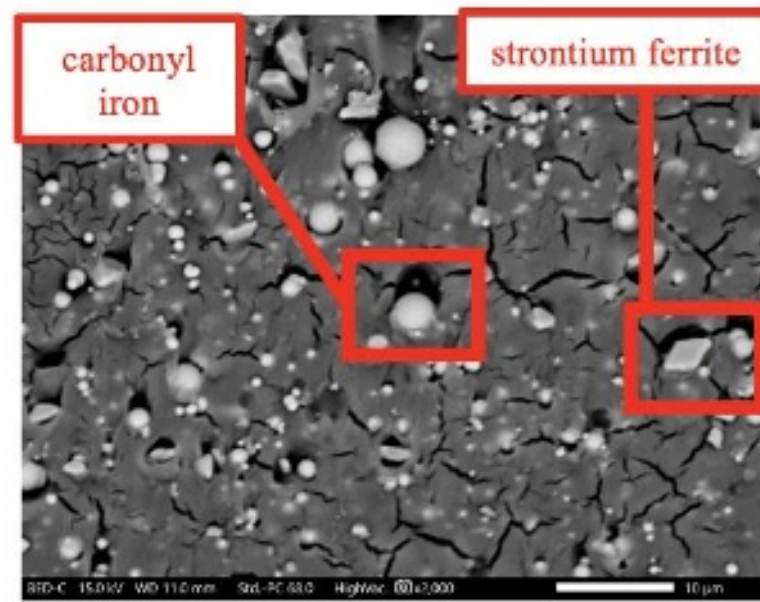


Figure 5 SEM image (10 micron scale bar) of 5SrF-10Fe-0M sample showing the two types of magnetic particulates within the filament. Both the carbonyl iron and strontium ferrite particulate appear brighter due to the higher Z elements present compared to the polymer matrix.

In general, SEM imaging reveals good dispersion of the particulate. There are not large agglomerations, but there is some local stratification within some samples. Figure 6 demonstrates these patterns, which were seen among all types of samples, regardless of percentages of strontium ferrite or carbonyl iron and regardless of magnetic annealing. These features may result from incomplete mixing of the particulate and/or attraction between the permanently magnetic SrF and soft magnetic iron particulate. It is clear from the properties observed in the magnetoactive results that there is a difference among the samples, but these SEM images do not provide the structural verification to explain the measured properties.

This is the author's peer reviewed, accepted manuscript. However, the online version of record will be different from this version once it has been copyedited and typeset.

PLEASE CITE THIS ARTICLE AS DOI:10.1063/1.50119669

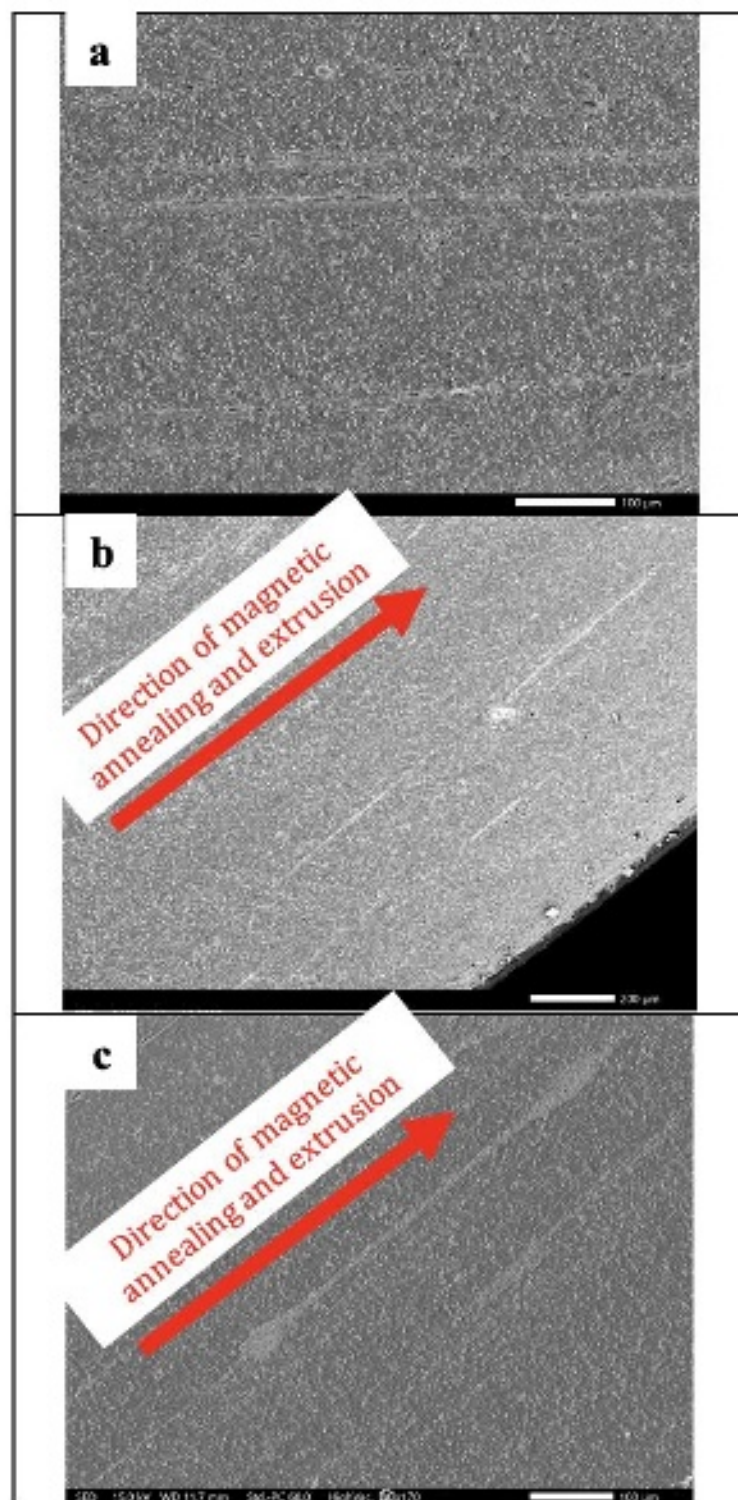


Figure 6 SEM Images (a) The 15SrF-0M sample (100 micron scale bar). (b) The 10SrF-5Fe- 5M sample (200 micron scale bar). (c) The 5SrF-10Fe-5M sample (100 micron scale bar). Stratification seen inconsistently throughout a range of samples.

V. Conclusion

This research created and analyzed filament with hard magnetic particulate for use in 3D printing via Fused Deposition Modeling (FDM). It investigated how magnetic annealing and the addition of soft magnetic iron influence the resulting magnetic and magnetoactive properties. Magnetic testing indicated that the magnetic properties of the SrF and Fe (coercive field, remnant magnetization, saturation magnetization) are transferred to the corresponding composite and smoothly combined, indicating the presence of magnetic coupling. The magnetoactive testing indicated that both magnetic annealing and increasing Fe percentage increase the magnetoactive response of the filament for the fields measured. Specifically, for the pure hard magnet SrF samples, magnetic annealing was essential to achieving magnetoactive deflection. Additionally, adding greater amounts of magnetically soft iron particulate increased the magnetoaction, but also resulted in a fairly soft magnetic composite. The SEM imaging indicated that there are shape differences between the SrF and Fe particulate, which likely has implications for magnetic properties. There is also a stratification effect along the extrusion direction, but it is not possible to distinguish the stratification causes between different types of samples. Further analysis and innovation of the structural composition of magnetic elastomers could lead to a better understanding of these complex smart materials.

VI. Acknowledgements

We would like to thank the Undergraduate Research Opportunities Program at the University of St. Thomas (UST) for partial funding of this project. We thank Professor Bethany Stadler at the University of Minnesota (UMN) for access to the equipment used to collect magneto-mechanical data, and Alex Robinson from UST for assistance in capturing qualitative images for the magneto-mechanical data collection. Part of this work was made possible with support from the National Science Foundation under Grant No. 2018344. Part of this work was performed at the Institute for Rock Magnetism (IRM) at UMN. The IRM is a US National Multi-user Facility supported through the Instrumentation and Facilities program of the National Science Foundation, Earth Sciences Division, and by funding from UMN.

References:

- 1) Y. Kim and X. Zhao. Chem. Rev. 122, 5317 (2022).
<https://doi.org/10.1021/acs.chemrev.1c00481>, [Google Scholar](#), [Crossref](#)
- 2) A.K. Bastola, M. Paudel, and L. Li. Polymer. 149, 213-228 (2018).
<https://doi.org/10.1016/j.polymer.2018.06.076>, [Google Scholar](#), [Crossref](#)
- 3) E. Dohmen, A. Saloum, and J. Abel. Philosophical Transactions of the Royal Society A. 378 (2020). <https://doi.org/10.1098/rsta.2019.0257>, [Google Scholar](#), [Crossref](#)
- 4) Z. Varga, G. Filipcsei, and M. Zrínyi. Polymer. 46, 13, 7779-7787 (2005).
<https://doi.org/10.1016/j.polymer.2005.10.139>, [Google Scholar](#), [Crossref](#)
- 5) S.S. Kang, K. Choi, J.D. Nam, and H.J. Choi. Materials. 13 (2020).
<https://doi.org/10.3390/ma13204597>, [Google Scholar](#), [Crossref](#)

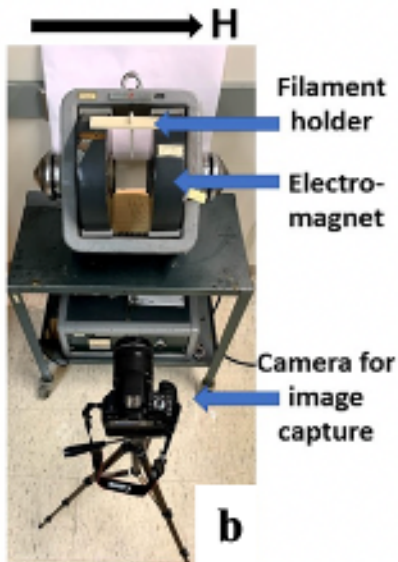
- 6) Y. Li, J. Li, W. Li, and H. Du. IOP Science Smart Materials and Structures. 23, 12 (2014). <https://doi.org/10.1088/0964-1726/23/12/123001>, [Google Scholar](#), [Crossref](#)
- 7) J. Yang, S. Sun, X. Yang, Y. Ma, G. Yun, R. Chang, S. Tang, M. Nakano, Z. Li, H. Du, S. Zhang, and W. Li. IEEE/ASME Transactions of Mechatronics. (2022). <https://doi.org/10.1109/TMECH.2022.3157329>, [Google Scholar](#), [Crossref](#)
- 8) M. Suppan, C. Huber, K. Mathauer, C. Abert, F. Brucker, J. Gonzalez-Gutierrez, S. Schuschnigg, M. Groenefeld, I. Teliban, S. Kobe, B. Saje, and D. Suess. SSRN Electronic Journal (2022). <https://dx.doi.org/10.2139/ssrn.4012463>, [Google Scholar](#), [Crossref](#)
- 9) C. Huber, S. Cano, I. Teliban, S. Schuschnigg, M. Groenefeld, and D. Suess. AIP Advances. 127, 063904 (2020). <https://doi.org/10.1063/1.5139493>, [Google Scholar](#), [Crossref](#)
- 10) A.H. Morgenstern, T.M. Calascione, N.A. Fischer, T.J. Lee, J.E. Wentz, and B.B. Nelson-Cheeseman. AIMS Materials Science. 6, 363 (2019). <https://doi.org/10.3934/matricsci.2019.3.363>, [Google Scholar](#), [Crossref](#)
- 11) N.A. Fischer, A.L. Robinson, T.J. Lee, T.M. Calascione, L. Koerner, and B.B. Nelson-Cheeseman. Journal of Magnetism and Magnetic Materials. 553 (2022). <https://doi.org/10.1016/j.jmmm.2022.169266>, [Google Scholar](#), [Crossref](#)
- 12) P. von Lockette, S.E. Lofland, J. Biggs, J. Roche, J. Mineroff, and M. Babcock. IOP Science Smart Materials and Structures. 20, 10 (2011). <https://doi.org/10.1088/0964-1726/20/10/105022>, [Google Scholar](#), [Crossref](#)
- 13) Y. Kim, H. Yuk, R. Zhao, S. Chester, and X. Zhao. Nature. 558, 274-279 (2018). <https://doi.org/10.1038/s41586-018-0185-0>, [Google Scholar](#), [Crossref](#)
- 14) T. M. Calascione, N.A. Fischer, T.J. Lee, H.G. Thatcher, and B.B. Nelson-Cheeseman. AIP Advances. 11, 025223 (2021). <https://doi.org/10.1063/9.0000220>, [Google Scholar](#), [Crossref](#)
- 15) A.K. Bastola, V.T. Hoang, and L.Li. Materials and Design. 114, 391-397 (2017). <https://doi.org/10.1016/j.matdes.2016.11.006>, [Google Scholar](#), [Crossref](#)
- 16) N. Bira, P. Dhagat, and J. R. Davidson. Frontiers in Robotics and AI. 7, 588391 (2020). <https://doi.org/10.3389/frobt.2020.588391>, [Google Scholar](#), [Crossref](#)
- 17) R. Zhao, Y. Kim, S. Chester, P. Sharma, and X. Zhao. Journal of the Mechanics and Physics of Solids. 124, 244-263 (2019). <https://doi.org/10.1016/j.jmps.2018.10.008>, [Google Scholar](#), [Crossref](#)

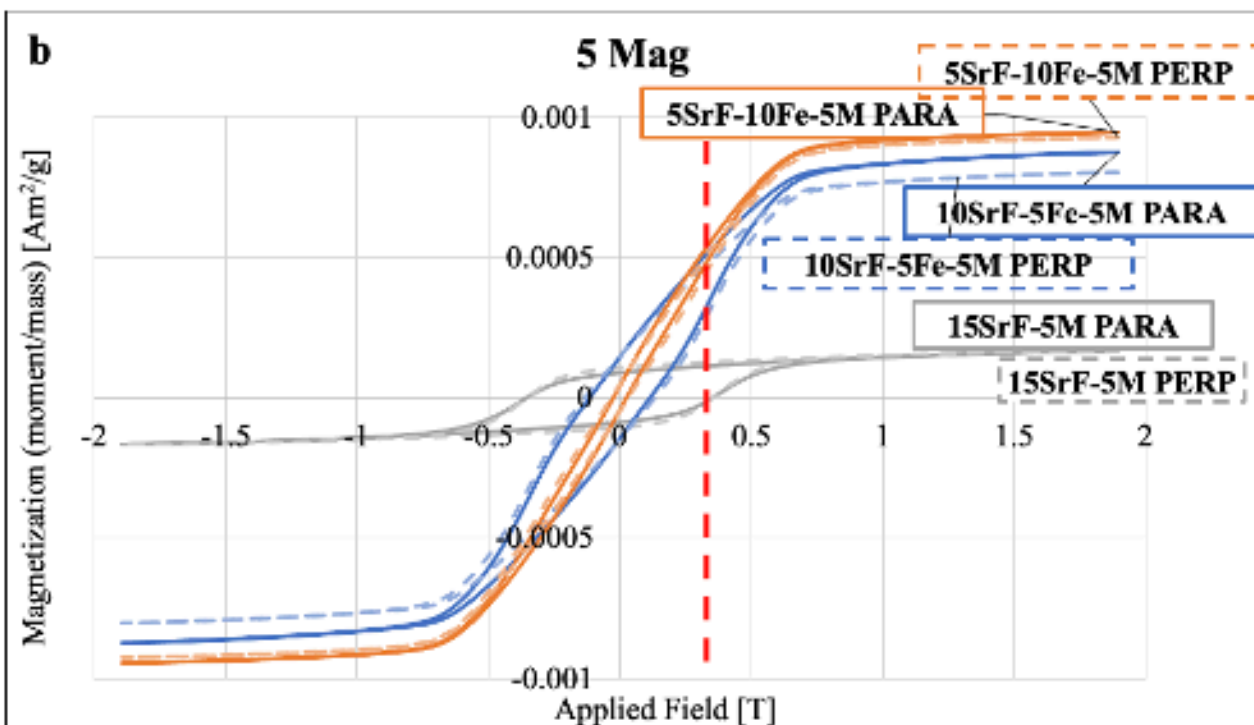
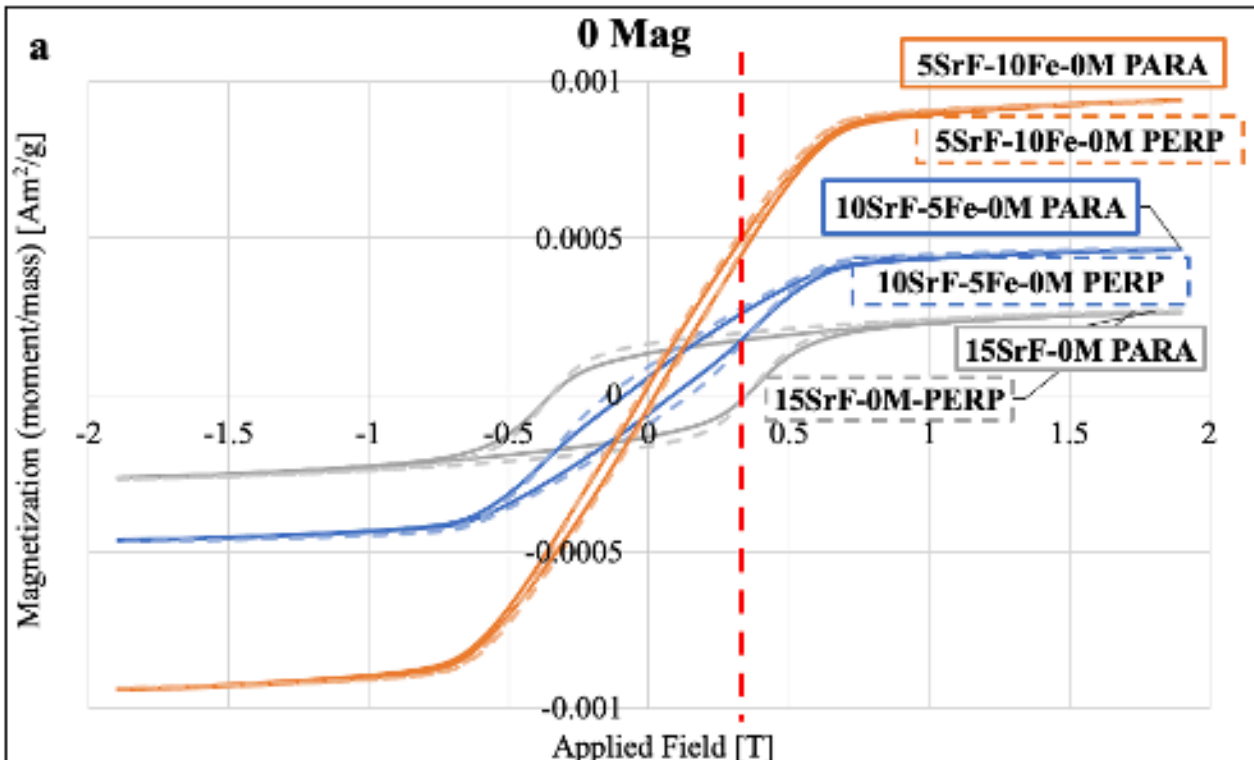
- 18) E.Y. Kramarenko, A.V. Chertovich, G.V. Stepanov, A.S. Semisalova, L.A. Makarova, N.S. Perov, and A.R. Khokhlov. *Smart Materials and Structures*. 24, 3 (2015). <https://doi.org/10.1088/0964-1726/24/3/035002>, [Google Scholar](#), [Crossref](#)
- 19) L.A. Makarova, Y.A. Alekhina, and N.S. Perov. *Journal of Magnetism and Magnetic Materials*. 440, 30-32 (2017). <https://doi.org/10.1016/j.jmmm.2016.12.095>, [Google Scholar](#), [Crossref](#)
- 20) N.M. Ardehali, M. Hemmatian, and R. Sedaghati. *Journal of Intelligent Material Systems and Structures*. 32, 9 (2020). <https://doi.org/10.1177/1045389X20942569>, [Google Scholar](#), [Crossref](#)
- 21) Q. Wen, Y. Wang, and X. Gong. *Smart Materials and Structures*. 26, 7 (2017). <https://doi.org/10.1088/1361-665X/aa7396>, [Google Scholar](#), [Crossref](#)
- 22) J. Koo, A. Dawson, and H. Jung. *Journal of Intelligent Material Systems and Structures*. 23,9 (2012). <https://doi.org/10.1177/1045389X12439635>, [Google Scholar](#), [Crossref](#)
- 23) G.V. Stepanov, D.Y. Borin, A.V. Bakhtiarov, and P.A. Storozhenko. *Smart Materials and Structures*. 26, 3 (2017). <https://doi.org/10.1088/1361-665X/aa5d3c>, [Google Scholar](#), [Crossref](#)
- 24) M. Przybylski, B. Ślusarek, T. Bednarczyk, and G. Chimel. *ACTA Physica Polonica A*. 136, 685-688 (2019). <https://doi.org/10.12693/APhysPolA.136.685>, [Google Scholar](#), [Crossref](#)
- 25) E. Palmero, D. Casaleiz, N. Jiménez, J. Rial, J. de Vicente, A. Nieto, R. Altimira, and A. Bollero. *IEEE Transactions of Magnetics*. 55, 2 (2019). <https://doi.org/10.1109/TMAG.2018.2863560>, [Google Scholar](#), [Crossref](#)
- 26) M. El Yaagoubi, M. Schrödl, D. Schwegler, and B. Münster. *Sensors and Actuator A: Physical*. 333 (2022). <https://doi.org/10.1016/j.sna.2021.113224>, [Google Scholar](#), [Crossref](#)
- 27) M. El Yaagoubi, S. Haas, and D. Schwegler. *Polymer Engineering and Science*. 61, 11 (2021). <https://doi-org.ezp2.lib.umn.edu/10.1002/pen.25801>, [Google Scholar](#), [Crossref](#)
- 28) D. Li, F. Wang, A. Xia, L. Zhang, T. Li, C. Jin, and X. Liu. *Journal of Magnetism and Magnetic Materials*. 417, 355-358 (2016) <https://doi.org/10.1016/j.jmmm.2016.05.094>, [Google Scholar](#), [Crossref](#)
- 29) T.J. Lee, A. Morgenstern, T. Höft, and B.B. Nelson-Cheeseman. *AIMS Materials Science*. 6, 3, 354-362 (2019). <https://doi.org/10.3934/matricsci.2019.3.354>, [Google Scholar](#), [Crossref](#)

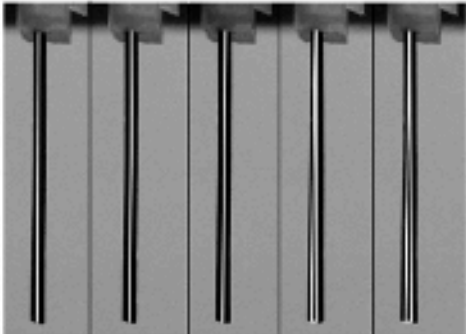
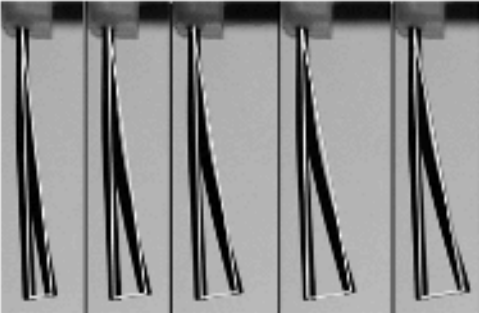

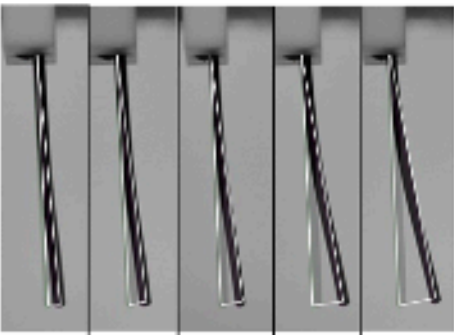
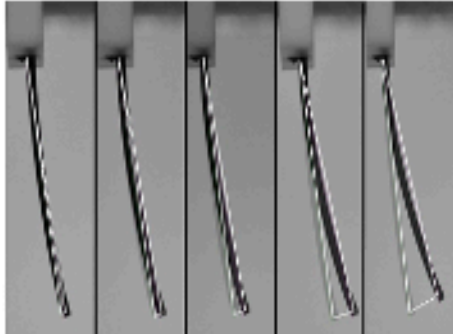
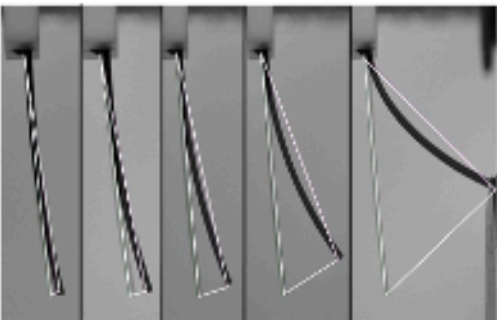
This is the author's peer reviewed, accepted manuscript. However, the online version of record will be different from this version once it has been copyedited and typeset.

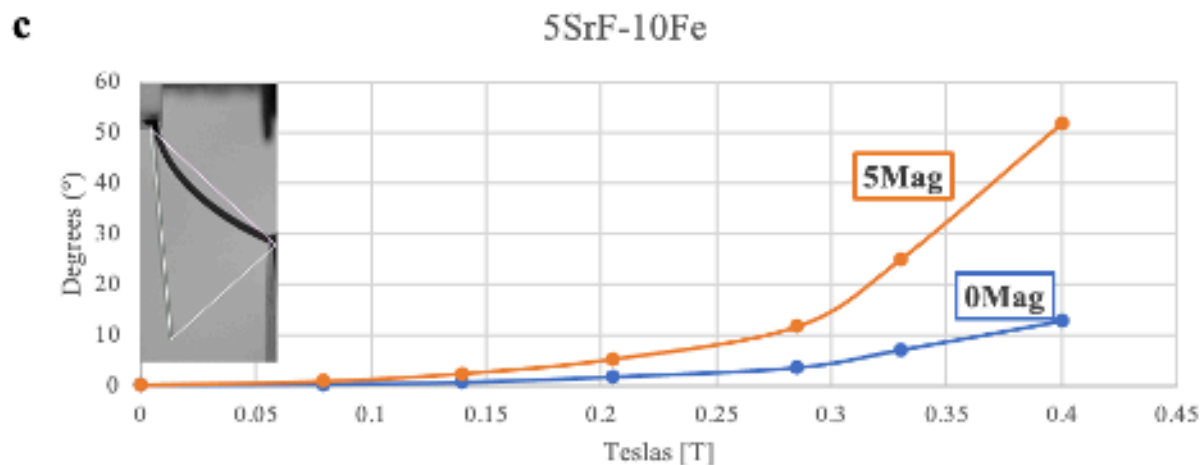
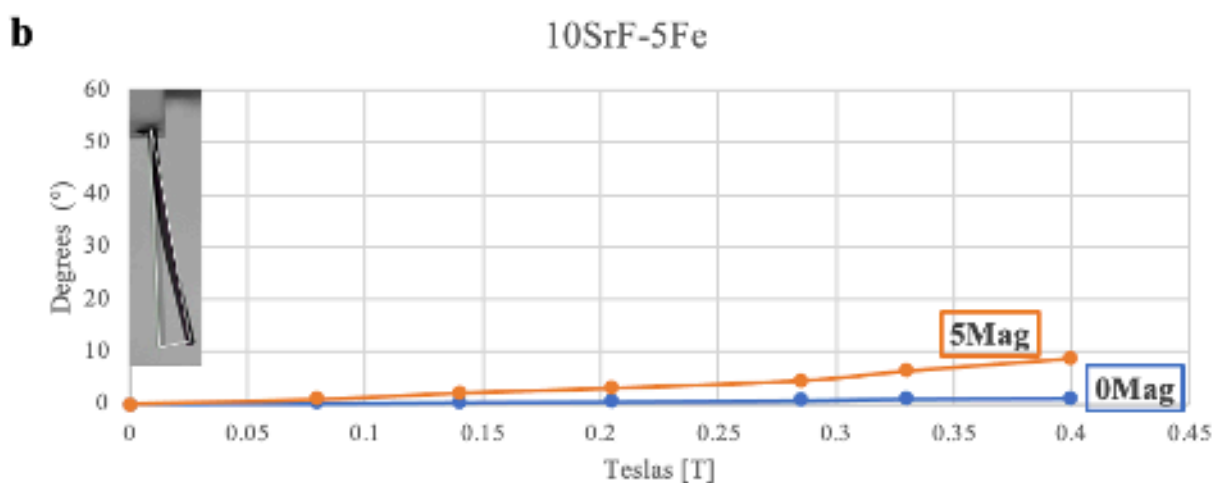
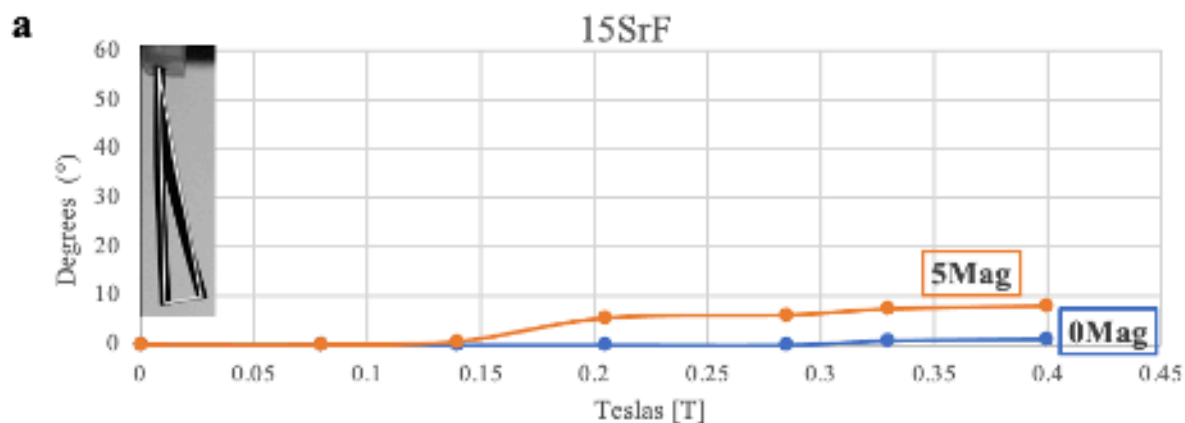
PLEASE CITE THIS ARTICLE AS DOI:10.1063/1.50119669

- 30) B.D. Cullity and C.D. Graham. Introduction to Magnetic Materials. Reading, Massachusetts, Addison-Wesley (1972).



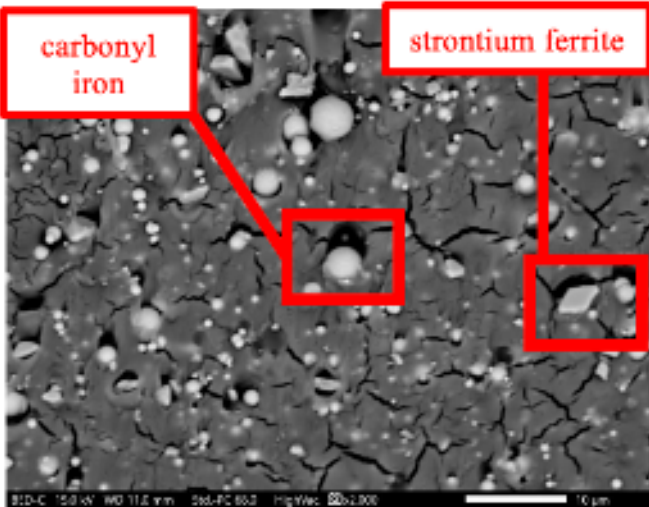


	0 MAG	5 MAG
15SrF	<p><i>15 SrF- 0 Mag</i></p>  <p>0.140 T 0.205 T 0.285 T 0.330 T 0.400 T</p>	<p><i>15 SrF- 5 Mag</i></p>  <p>0.140 T 0.205 T 0.285 T 0.330 T 0.400 T</p>
10SrF-5Fe	<p><i>10SrF-5Fe-0Mag</i></p>  <p>0.140 T 0.205 T 0.285 T 0.330 T 0.400 T</p>	<p><i>10SrF-5Fe-5Mag</i></p>  <p>0.140 T 0.205 T 0.285 T 0.330 T 0.400 T</p>
5SrF-10Fe	<p><i>5SrF-10Fe-0Mag</i></p>  <p>0.140 T 0.205 T 0.285 T 0.330 T 0.400 T</p>	<p><i>5SrF-10Fe-5Mag</i></p>  <p>0.140 T 0.205 T 0.285 T 0.330 T 0.400 T</p>

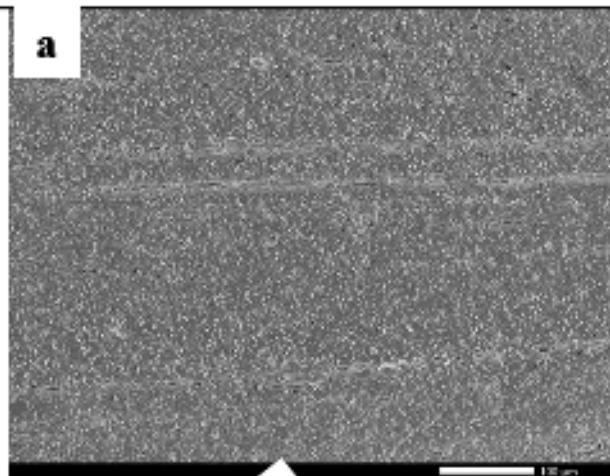


carbonyl
iron

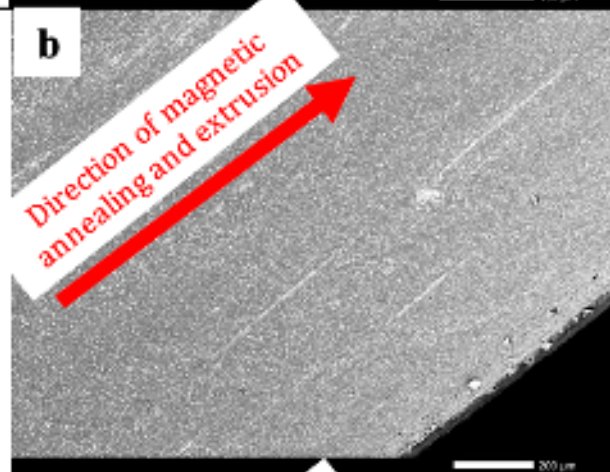
strontium ferrite



a



b



c

